ACS OMEGA

Open Access

http://pubs.acs.org/journal/acsodf

Article

Development of a New Class of Monoamine Oxidase-B Inhibitors by Fine-Tuning the Halogens on the Acylhydrazones

Jayalakshmi Jayan,◆ Jiseong Lee,◆ Sunil Kumar, Amritha Manoharan, Anishma Payyappilliparambil Narayanan, Reenoo Jauhari, Mohamed A. Abdelgawad, Mohammed M. Ghoneim, Hasnaa Ali Ebrahim, Subin Mary Zachariah,* Hoon Kim,* and Bijo Mathew*

Cite This: *ACS Omega* 2023, 8, 47606−47615

Read Online

ACCESS | Metrics & More | Article Recommendations | Supporting Information

ABSTRACT: A total of 14 acyl hydrazine derivatives (**ACH1**−**ACH14**) were developed and examined for their ability to block monoamine oxidase (MAO). Thirteen analogues showed stronger inhibition potency against MAO-B than MAO-A. With a half-maximum inhibitory concentration of 0.14 μM, **ACH10** demonstrated the strongest inhibitory activity against MAO-B, followed by **ACH14**, **ACH13**, **ACH8**, and **ACH3** (IC_{50} = 0.15, 0.18, 0.20, and 0.22 μM, respectively). Structure−activity relationships suggested that the inhibition effect on MAO-B resulted from the combination of halogen substituents of the A- and/or B-rings. This series concluded that when −F was substituted to the B-ring, MAO-B inhibitory activities were high, except for **ACH6**. In the inhibition kinetics study, the compounds **ACH10** and **ACH14** were identified as competitive inhibitors, with K_i values of 0.097 ± 0.0021 and 0.10 ± 0.038 μM, respectively. In a reversibility experiment using the dialysis methods, **ACH10** and **ACH14** showed effective recoveries of MAO-B inhibition as much as lazabemide, a reversible reference. These experiments proposed that **ACH10** and **ACH14** were efficient, reversible competitive MAO-B inhibitors. In addition, the lead molecules showed good blood−brain barrier permeation with the PAMPA method. The molecular docking and molecular dynamics simulation study confirmed that the hit compound ACH10 can form a stable protein−ligand complex by forming a hydrogen bond with the NH atom in the hydrazide group of the compound.

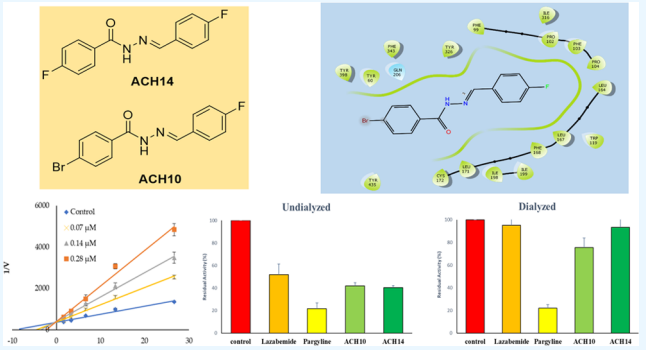

1. INTRODUCTION

The dietary and biogenic amines that form by breaking down food are metabolized by some essential mitochondrial enzymes. These are key isoenzymes known as monoamine oxidase (MAO) (i.e., MAO-A and MAO-B), exclusively found in the surface membrane.[1] A and B isoforms of MAO were isolated and thoroughly studied and found to display roughly 70% sequence identity.[2] Each type has a distinct tissue allocation strategy and substrate selectivity and is encoded by a different gene. The way these two enzymes selectively oxidize neurotransmitters is one of their primary distinctions. While the MAO-A enzyme preferentially oxidizes phenylethylamine,[3] the MAO-B enzyme selectively oxidizes neurotransmitters, such as norepinephrine and serotonin.[4] In contrast, both enzymes oxidize the neurotransmitter dopamine.[5] Reports from a limited number of past studies suggest that MAO-B may be responsible for dopamine breakdown.[6]

The onset and progression of many neurodegenerative disorders are significantly influenced by these MAO enzymes.[7] The majority of individuals worldwide are affected by the defect. Dementia or memory loss is the primary side effect of neurodegenerative conditions.[8] In contrast to static neuronal loss[9] caused by metabolic or toxic diseases, neurodegenerative disorders are distinguished by the gradual degeneration of groups of neuronal networks[10] that are particularly vulnerable to the disorders. Alzheimer's disease (AD) is one of the most common causes of the worsening of dementia.[11] Pathologically, AD is characterized by the emergence of extracellular senile plaques containing amyloid A proteins and intracellular neurofibrillary tangles.[12] Parkinson's disease (PD) is triggered due to the depletion of dopaminergic neurons in the area known as the substantia nigra, as well as the buildup of Lewy bodies, which are eosinophilic inclusion bodies.[13] Patients with PD and AD have significantly enhanced MAO-B expression and activity in their brains.[14]

MAO-A-blocking medications have been used to treat psychiatric disorders, such as depression and anxiolytic

Received: August 4, 2023
Revised: November 21, 2023
Accepted: November 24, 2023
Published: December 6, 2023

Scheme 1. Reagents and Conditions: (a) Microwave, 200 °C, 10−15 min; (b) Microwave, Glacial Acetic Acid, 60−80 °C, 20−30 min

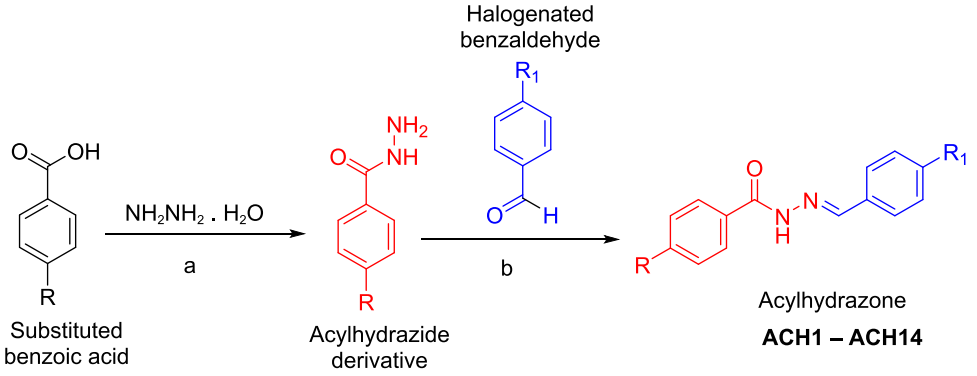

disorders,[15] because MAO-A is a protein that breaks down noradrenaline and serotonin in the central nervous system (CNS).[16] MAO-B inhibitors have been used to treat neurodegenerative disorders, including PD and AD, because MAO-B is an essential CNS enzyme for the metabolism of phenylethylamine and dopamine.[17] MAO-B inhibitors are regarded to be viable therapeutic agents for PD and AD because they can increase dopamine levels while reducing the formation of reactive oxygen species.[18]

Many scaffolds, such as coumarins, isatins, chalcones, and hydrazones, are used to target both MAO-A and MAO-B.[19−23] This particular research focuses on the hydrazone moiety, which has been widely reported to inhibit MAO-B activity. The N-acylhydrazone moiety can serve as a ligand for various receptor types. Due to the coupling of its acyl and imine molecules to other subunits, it undergoes several changes that control a range of molecular targets.[24]

Hydrazones are created when a hydrazine molecule interacts with a carbonyl functional group in the presence of an acid catalyst. The −C═N−NH− group, which is present in hydrazone derivatives, is crucial in the search for novel therapeutic compounds. The structural cores of hydrazones, which include two distinctly linked nitrogen atoms, often regulate their physical and chemical characteristics.[25] Hydrazones are frequently used to produce distinctive compounds with a variety of activities. Studies have reported halogens being inserted into the structure of acylhydrazone to produce halogenated acylhydrazone derivatives.[26] The FDA-approved MAO-B inhibitors such as safinamide frequently include halogens, which are electron-withdrawing groups, within their structure.[27] Halogens enhance protein−ligand interaction in the MAO cavity and promote blood−brain barrier (BBB) permeability.[28] The hydrazide-hydrazone moiety interacts with MAO enzymes more favorably and inhibits MAO-B competitively and reversibly.[29]

In this study, 14 halogenated acylhydrazone variants were produced. MAO-A and MAO-B inhibitory studies were performed for all of these compounds. Some of the molecules exhibited (lead molecules) promising activity, for which kinetic and reversibility studies were performed. To learn more about the mode and capability of the lead compounds that inhibit MAO-A and MAO-B proteins, molecular docking studies were conducted. To describe the protein−peptide complexes, molecular dynamics (MD) simulations were used to further validate the docking data.

2. MATERIALS AND METHODS

2.1. Chemicals. Recombinant human MAO-A and MAO-B, benzylamine, kynuramine, lazabemide, pargyline, clorgyline, and toloxatone were purchased from Sigma-Aldrich (St. Louis, MO). Sodium phosphate (dibasic and monobasic anhydrous) was purchased from Daejung (Siheung, Korea). Dialyzer (6−8 kDa, DiaEasy) was purchased from BioVision (St. Grove, MA).[30]

2.2. Synthesis of Acylhydrazide. In the first step, 1 equiv of both plain and halogenated benzoic acid was taken and reacted with 3 equiv of hydrazine hydrate under microwave (Monowave 50, Anton Paar, Graz, Austria) conditions. The temperature was set up to 200 °C, and the reaction time was 10−15 min. The acylhydrazides with and without halogen substitutions were obtained, filtered, and recrystallized using ethanol to obtain pure solid crystals.

2.3. Synthesis of Acylhydrazone. The *para*-substituted benzaldehyde was mixed in an equimolar ratio with the intermediate molecules (acylhydrazide derivatives) in ethyl alcohol. A few drops of glacial acetic acid were introduced into the reacting mixture and were permitted to react for 20−30 min at 60−80 °C under microwave conditions.[31,32] The final target molecule was obtained, which was then filtered and dried. After each step, the purity and success of the reaction of the produced compounds were examined by using thin-layer chromatography (TLC). The solvent system for the TLC consisted of hexane and ethyl acetate in a 2:1 ratio.

The synthetic scheme for acylhydrazide and acylhydrazones is represented in Scheme 1, and the structures of the compounds are represented in Figure 1.

2.4. Enzyme Assays. The activity levels of MAO-A and MAO-B were investigated for 30 min at 25 °C by continuously monitoring the change in absorbance at 316 and 250 nm, respectively, for the respective substrate kynuramine (0.06 mM) and benzylamine (0.30 mM), in 0.5 mL of reaction mixture containing 50 mM sodium phosphate (pH 7.2). Reactions were started by the addition of the substrate to the enzyme mixtures. K_m values were determined at five distinct levels of substrate concentrations (0.0075−0.12 and 0.0375−0.60 μM, respectively).[33]

2.5. Inhibition Studies. Residual activity was assayed after the addition of the 10 μM inhibitor as an initial screening step; IC_{50} values were then determined for potential compounds with residual activity of less than 50% using residual activity curves obtained by GraphPad Prism software 5 (San Diego, CA).[34] By dividing the IC_{50} of MAO-A with that of MAO-B,

https://doi.org/10.1021/acsomega.3c05719
ACS Omega 2023, 8, 47606−47615

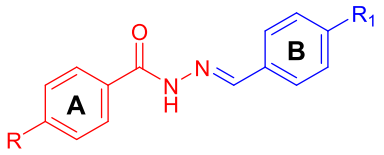

CODE	R	R1	CODE	R	R1
ACH1	–H	–Cl	ACH8	–Br	–Cl
ACH2	–H	–Br	ACH9	–Br	–Br
ACH3	–H	–F	ACH10	–Br	–F
ACH4	–Cl	–Cl	ACH11	–Br	–H
ACH5	–Cl	–Br	ACH12	–F	–Cl
ACH6	–Cl	–F	ACH13	–F	–Br
ACH7	–Cl	–H	ACH14	–F	–F

Figure 1. Structure of **ACH** compounds.

the selectivity index (SI) value of MAO-B was determined.[35] The types of inhibition exerted by the leading compounds for MAO-A and MAO-B were determined at the five substrate concentrations and three distinct inhibitory concentrations (~0.5×, 1.0×, and 2.0× IC_{50}).[36] Toloxatone, chlorobenzene, lazabemide, and pargyline were used as reference compounds. Lineweaver–Burk plot and secondary plot comparisons were used for establishing enzyme kinetic patterns and K_i values, respectively.[37]

2.6. Reversibility Studies. The ability of the leading compounds to reverse MAO-A and MAO-B activity was evaluated by comparing undialyzed and dialyzed residual activities at a concentration roughly twice the IC_{50} after preincubation for 30 min prior to measurement, as previously described.[38] Two types of reference inhibitors were used: reversible blockers toloxatone (MAO-A) and lazabemide (MAO-B) and irreversible inhibitors clorgyline (MAO-A) and pargyline (MAO-B). Reversibility patterns were identified through the comparison of the behaviors of undialyzed (A_U) and dialyzed (A_D) samples, taking the reference results into account.

2.7. Blood–Brain Barrier (BBB) Permeability Assay. BBB permeability is a very important criterion for the compounds targeting CNS delivery. To examine BBB permeability for the leading compounds, an *in vitro* permeation assay, named parallel artificial membrane permeability assay (PAMPA), was carried out. PAMPA, a non-cell-based assay, is used to forecast a drug's passive and transcellular permeability across the BBB. In PAMPA, a 96-well microplate and a 96-well Millipore filter plate (IPVH, 125 μm thick filter, 0.45 μm pore) were sandwiched together and then soaked in 4 μL of *n*-dodecane. Prior to use, these stock solutions of the compounds were kept to 10 mM in DMSO at 0 °C. The stock solution was initially diluted with buffer to get a final concentration of 1, 0.1, and 0.01 mM, lowering the DMSO content below 1% (v/v), before being placed on a 96-well filter plate.

The effective permeability (Pe) of the compounds was calculated by the following equation

$$\mathrm{Pe} = -\ln[1 - A_R/\mathrm{equilibrium}]/A(1/V_D + 1/V_A)t$$

where Pe is the effective permeability (cm/s); A is the effective filter area (0.45 cm^2); A_R is the absorbance in receptor compartment; A_D is the absorbance in donor compartment; V_D is the volume of donor; V_A is the volume of acceptor (mL) and; t is time (s); equilibrium = (CDXVD + CAXVA)/(V_D + V_A).

2.8. Molecular Docking. We cautiously obtained the crystalline structure of MAO-primary B from the Protein Data Bank (PDB ID: 2V5Z, Resolution: 1.60 Å). Before selecting the PDB ID, we thoroughly investigated the literature. Chain A (499 residues) and Chain B (494 residues) are the two chains that make up this enzyme.[39,40] This PDB can be used to

Table 1. Inhibitions of MAO-A and MAO-B by Acyl Hydrazine Derivatives[a]

	residual activities at 10 μM (%)		IC50 (μM)		
compound	MAO-A	MAO-B	MAO-A	MAO-B	SI
ACH1	96.00 ± 8.49	10.71 ± 2.52	>40	0.36 ± 0.04	111.11
ACH2	130.74 ± 2.90	30.20 ± 0.95	>40	1.65 ± 0.21	24.24
ACH3	109.00 ± 7.07	7.08 ± 1.25	>40	0.22 ± 0.02	181.82
ACH4	92.11 ± 1.86	20.23 ± 1.68	>40	0.37 ± 0.006	108.11
ACH5	70.59 ± 4.16	35.84 ± 1.88	>40	1.54 ± 0.04	25.97
ACH6	117.11 ± 1.86	46.42 ± 1.68	>40	8.0 ± 0.037	5.00
ACH7	127.05 ± 3.48	43.55 ± 4.56	>40	12.8 ± 0.026	3.13
ACH8	59.56 ± 3.12	18.30 ± 3.45	20.22 ± 0.57	0.20 ± 0.09	101.10
ACH9	101.32 ± 1.86	98.22 ± 0.00	>40	>40	
ACH10	61.76 ± 6.24	11.74 ± 1.42	23.42 ± 0.56	0.14 ± 0.011	167.29
ACH11	102.46 ± 4.64	38.96 ± 5.61	>40	5.2 ± 0.056	7.69
ACH12	37.65 ± 2.24	33.77 ± 0.00	4.85 ± 0.83	5.6 ± 0.10	0.87
ACH13	38.46 ± 5.44	−50.85 ± 4.79	11.60 ± 0.07	0.18 ± 0.01	64.44
ACH14	63.75 ± 1.76	−14.41 ± 1.20	19.57 ± 1.41	0.15 ± 0.02	130.47
toloxatone			1.646 ± 0.094		
lazabemide				0.073 ± 0.0013	
clorgyline			0.0079 ± 0.00094		
pargyline				0.11 ± 0.011	

[a]Results are presented as mean ± standard errors of duplicate or triplicate experiments. Selectivity index (SI) values are expressed as IC_{50} for MAO-A/ IC_{50} for MAO-B.

https://doi.org/10.1021/acsomega.3c05719
ACS Omega 2023, 8, 47606–47615

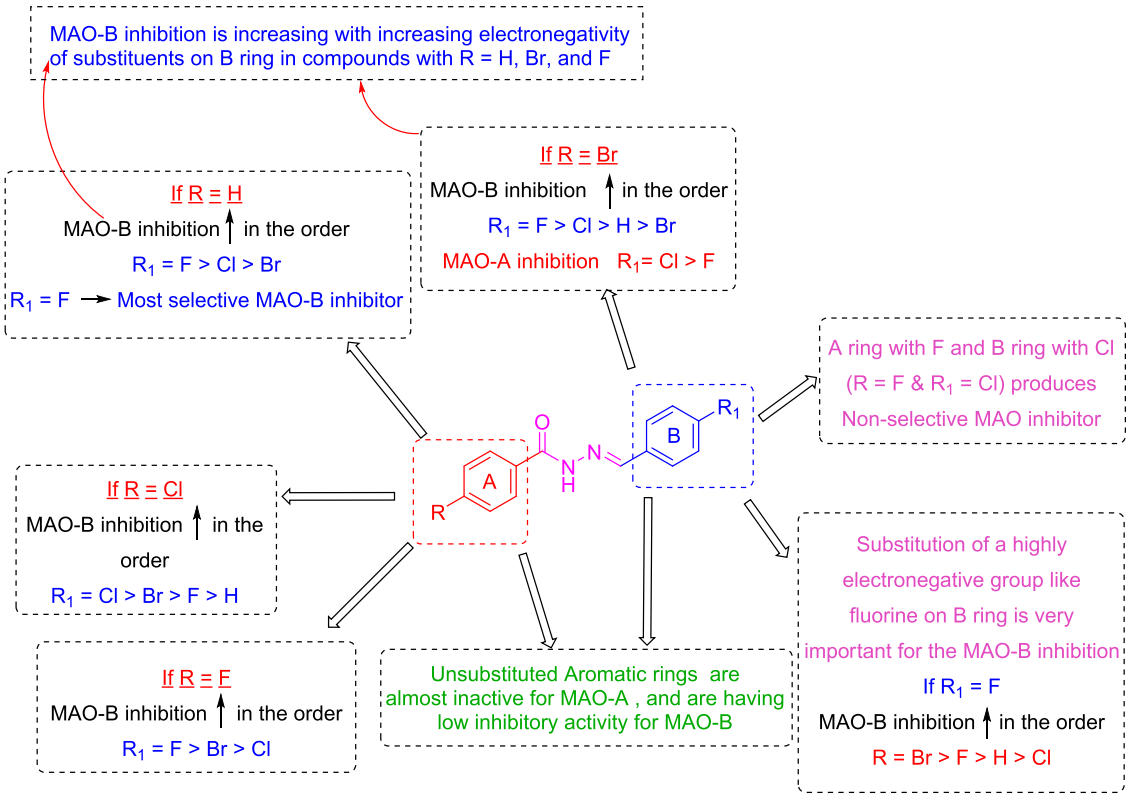

Figure 2. Structure−activity relationship of acylhydrazone-based MAO inhibition. MAO: monoamine oxidase.

import workflow in Maestro (Schrödinger Release 2021−4: Maestro, Schrödinger, LLC, New York, NY, 2021). By removing water molecules, changing side-chain protonation states, and providing missing hydrogen atoms, we optimized and reduced the crystal structures by employing the Protein Preparation Wizard application. The required protein was digested and further processed to make the grid. The centroid of the entering cocrystal ligand served as the default parameter for generating the grid. The Ligprep tool was used for getting the compounds ready for docking, and the OPLS-2005 force field was applied.[41]

2.9. Molecular Dynamics. The MD investigations for the least docking pose of compound ACH10 were executed using the Desmond package (Desmond V 7.2), which was installed on a Dell, Inc. Precision 7820 Tower with the following configuration: Ubuntu 22.04.1 LTS 64-bit, Intel Xenon silver 4210R, and NVIDIA Corporation GP104GL (RTX A 4000) graphics processing unit.[42] Even though the systems used the same parameters, earlier works[43−45] contain more information about the MD investigation (including solvent simulation box shape, size, barometer and thermostat parameters, and long- and short-range interaction calculations). The root-mean-square deviation (RMSD), root-mean-square fluctuation (RMSF), and protein−ligand interaction review, including every C atom, were generated to evaluate the domain correlations. Immediately after the MD run, 1000 frames of the selected MD trajectory were generated at 100 ps intervals to examine the dynamics of protein−ligand interaction.

3. RESULTS AND DISCUSSION

3.1. Chemistry. The desired compounds were synthesized in two stages. During the initial stage, the intermediate acylhydrazide molecule was synthesized by reacting benzoic acid and hydrazine hydrate. This intermediate molecule was then reacted with a different halogenated benzaldehyde to obtain the final molecules (halogenated acylhydrazone derivatives) by an acid-catalyzed nucleophilic addition reaction. All procedures were performed using a microwave reactor (Monowave 50, Anton Paar, Graz, Austria). The lead compound (**ACH10** and **ACH14**) structures were confirmed using ^{1}H, ^{13}C NMR (Bruker Avance Neo 500 MHz NMR spectrometer, Billerica, MA, USA), mass spectroscopy (Waters Xevo G2-XS QTOF, Milford, MA), and HPLC (Shimadzu Prominence-i LC-2030C 3D Plus, Ramsey, MN) (Supporting Information).

3.2. Inhibition Studies of MAO-A and MAO-B. Except for **ACH9**, the other 13 derivatives displayed a weak residual activity of less than 50% for MAO-B at a concentration of 10 μM, but only two compounds exhibited similar behavior for MAO-A (Table 1). **ACH10** showed the most potent suppressive efficacy against MAO-B, which possessed an IC_{50} value of 0.14 μM, followed by **ACH14** (IC_{50} = 0.15 μM), **ACH13** (IC_{50} = 0.18 μM), and **ACH3** (IC_{50} = 0.22 μM). In MAO-A, **ACH12** was the best inhibitor with an IC_{50} level of 4.85 μM, followed by **ACH13** (IC_{50} = 11.60 μM). In terms of selectivity index (SI), **ACH3** showed the highest SI value at 181.82, followed by **ACH10** (SI = 167.29). **ACH12** was identified as a nonspecific MAO inhibitor with an SI value of 0.87. If the cheese effect can be prevented through dietary advice, then nonspecific MAO inhibitors are excellent medications for the treatment of PD, depression, and drug resistance.[46,47]

ACH compounds were acylhydrazone derivatives containing a halogen group or a hydrogen atom bonded to a *para* site of A- and/or B-rings. **ACH10** and **ACH14**, the most potent compounds, had a highly electronegative −F substituent

https://doi.org/10.1021/acsomega.3c05719
ACS Omega 2023, 8, 47606−47615

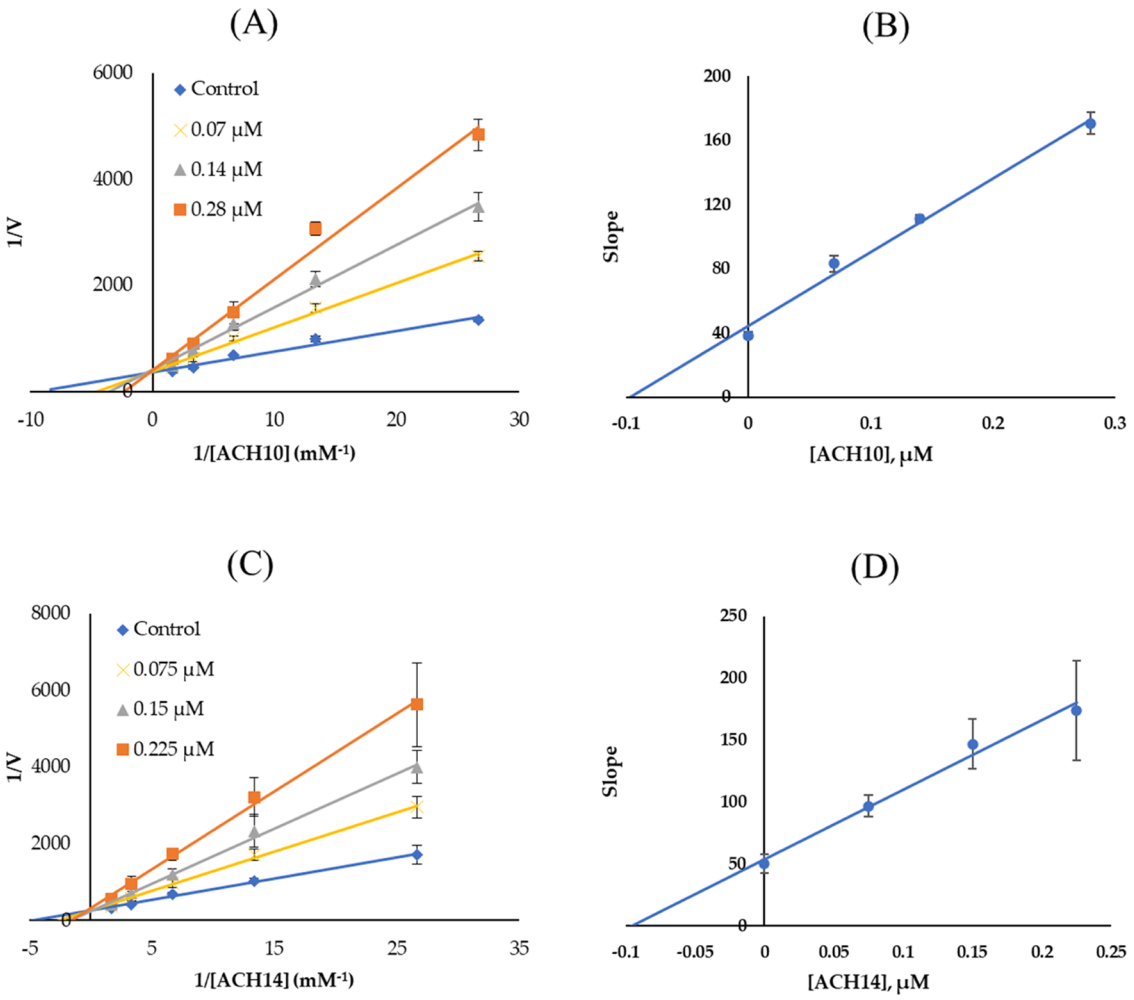

Figure 3. Lineweaver−Burk plots for MAO-B inhibitions by (A) **ACH10** and (C) **ACH14**, and the secondary plots (B and D, respectively) of the slopes vs inhibitor concentrations. MAO: monoamine oxidase.

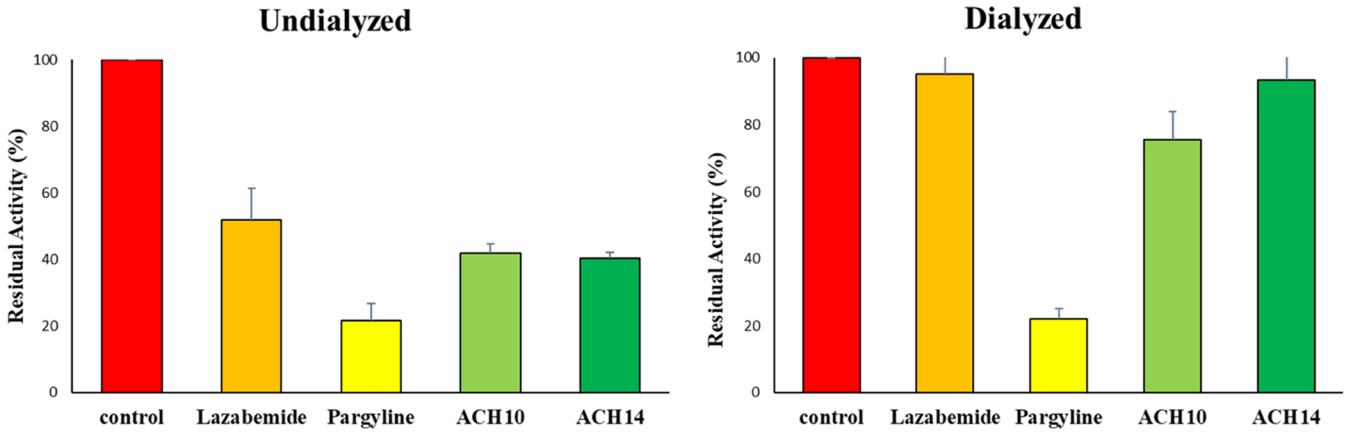

Figure 4. Recoveries of MAO-B inhibitions by **ACH10** and **ACH14** using dialysis experiments. MAO: monoamine oxidase.

Table 2. BBB Assay of ACH10 and ACH14 Using the PAMPA Method[a]

compound	Pe (cm/s)	prediction
ACH10	5.12×10^{-6}	CNS+
ACH14	4.98×10^{-6}	CNS+
selegiline	5.69 ± 0.04	CNS+

[a]Pe > 4.00×10^{-6} cm/s: CNS+ (high permeation).

bonded to a B-ring, with −Br and −F substituents in the A-ring, and increased the inhibitory activity (Table 1 and Figure 1). When comparing **ACH1**, **ACH2**, and **ACH3**, in which hydrogen was bonded to the A-ring, −F in the B-ring (**ACH3**) showed the strongest inhibitory ability, followed by −Cl (**ACH1**) and −Br (**ACH2**). However, when comparing **ACH4**, **ACH5**, **ACH6**, and **ACH7** substituted with −Cl in the A-ring, −Cl in the B-ring (**ACH4**) exhibited the strongest

https://doi.org/10.1021/acsomega.3c05719
ACS Omega 2023, 8, 47606−47615

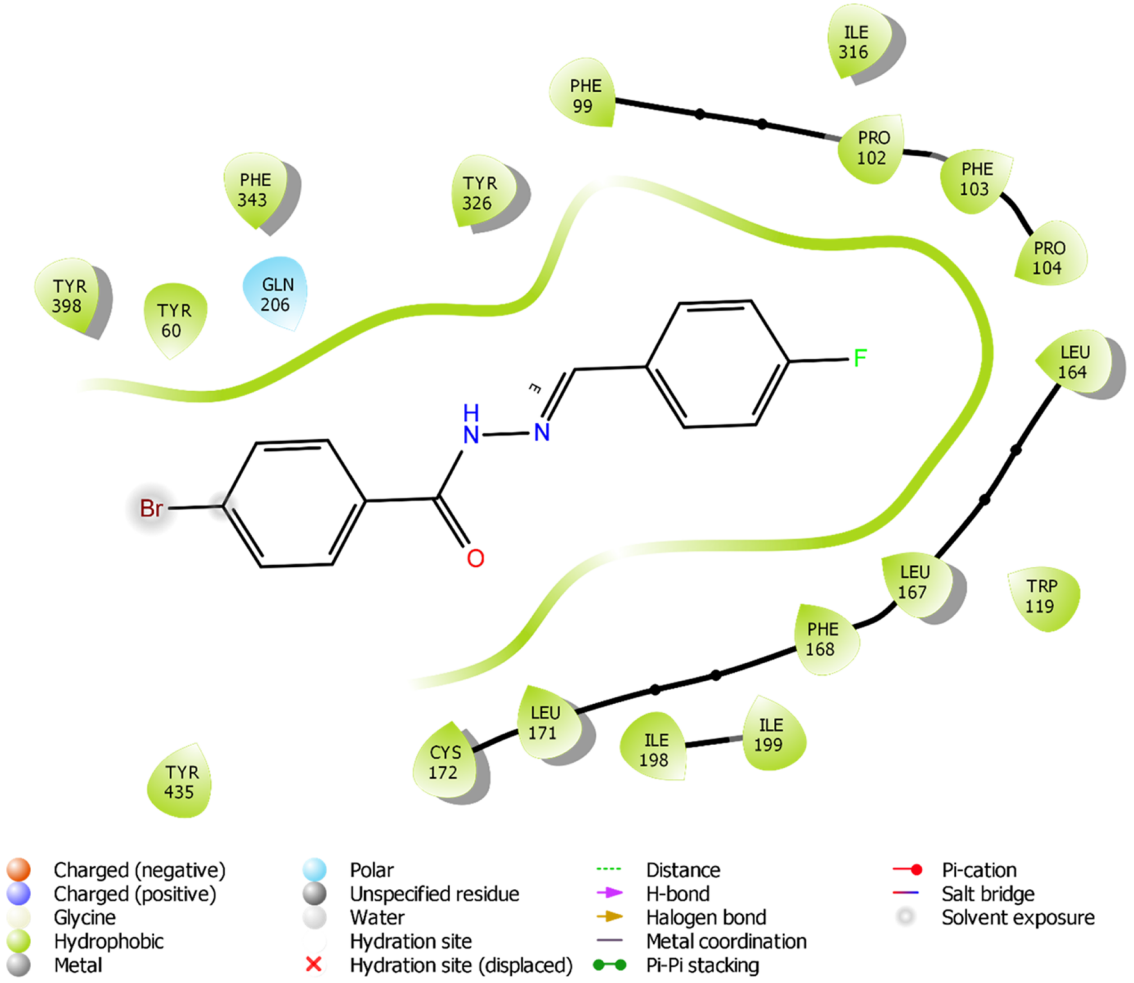

Figure 5. 2-D ligand interaction with lead compound **ACH10**.

inhibition of MAO-B, followed by **ACH5**, **ACH6**, and **ACH7**, such that −Cl > −Br > −*F* > −H, indicating that a particular electronegativity of substitution is important and the MAO-B antagonistic activity is reduced by increasing the electronegativity. When comparing **ACH8**, **ACH9**, **ACH10**, and **ACH11** substituted with −Br in the A ring, the inhibitory activities were effective in the order −F (**ACH10**) > −Cl (**ACH8**) > −H (**ACH11**) > −Br (**ACH9**). Interestingly, **ACH10** substituted with −F (the most electronegative group in the series) in the B-ring displayed a much stronger inhibitory activity against MAO-B than **ACH9** substituted with −Br in the B ring. Finally, when comparing **ACH12**, **ACH13**, and **ACH14** substituted with −F in the A-ring, −F (**ACH14**) in the B-ring exhibited the strongest inhibitory activity, followed by −Br (**ACH13**) and −Cl (**ACH12**). Specifically, when **ACH10** and **ACH13** were compared, it was observed that they had similar IC_{50} values even when the positions of the functional groups −F, or −Br were reversed. Additionally, when **ACH10** and **ACH14** were compared, a difference in substituents bound to the A ring (**ACH10** = −Br, **ACH14** = −F) showed similar IC_{50} levels. Collectively, it was suggested that the inhibition effect on MAO-B resulted in the combination of the halogen substituents of the A- and B-rings (Figure 2). In this series, it was concluded that when −F was substituted into the B ring, MAO-B inhibitory activities became high, except for **ACH6**. In addition, it can be interpreted that compound **ACH12** with higher activity for MAO-A inhibition with an IC_{50} value (4.85 μM), and all of the other derivatives showed values greater than 10 μM. Followed by **ACH12**, compounds **ACH13** (IC_{50} = 4.85 μM) and **ACH14** (IC_{50} = 19.57 μM) showed comparatively good activity against MAO-A. From the results, it is assumed that fluorine substitution on the A-ring (R = F) has a crucial role in the MAO-A inhibitory property.

3.3. Enzyme Kinetics. The enzyme kinetics and inhibition studies were conducted at five substrate concentrations and three different inhibitors (**ACH10** or **ACH14**). In the Lineweaver−Burk plot, **ACH10** and **ACH14** appeared to be competitive MAO-B inhibitors (Figure 3A,C). The K_i values obtained through secondary plots were 0.097 ± 0.0021 and 0.10 ± 0.038 μM, respectively (Figure 3B,D). These results suggested that **ACH10** and **ACH14** can act as potent competitive MAO-B inhibitors.

3.4. Reversibility Studies. Following a 30 min preincubation period, the ability to reverse the MAO-B inhibition by **ACH10** or **ACH14** could be determined by employing a dialysis method. For the assay, concentrations of **ACH10** and **ACH14** at twice their IC_{50} values (0.28 and 0.30 μM, respectively) were used. The recovery pattern was compared by using the A_U and dialyzed A_D proportional activities. The recovery of MAO-B inhibitory activity for **ACH10** was from 42.00 to 75.49%, and that for **ACH14** was from 40.37 to 93.40% (Figure 4). The recovery rates of the compounds seemed to be comparable to that of lazabemide (reversible

https://doi.org/10.1021/acsomega.3c05719
ACS Omega 2023, 8, 47606−47615

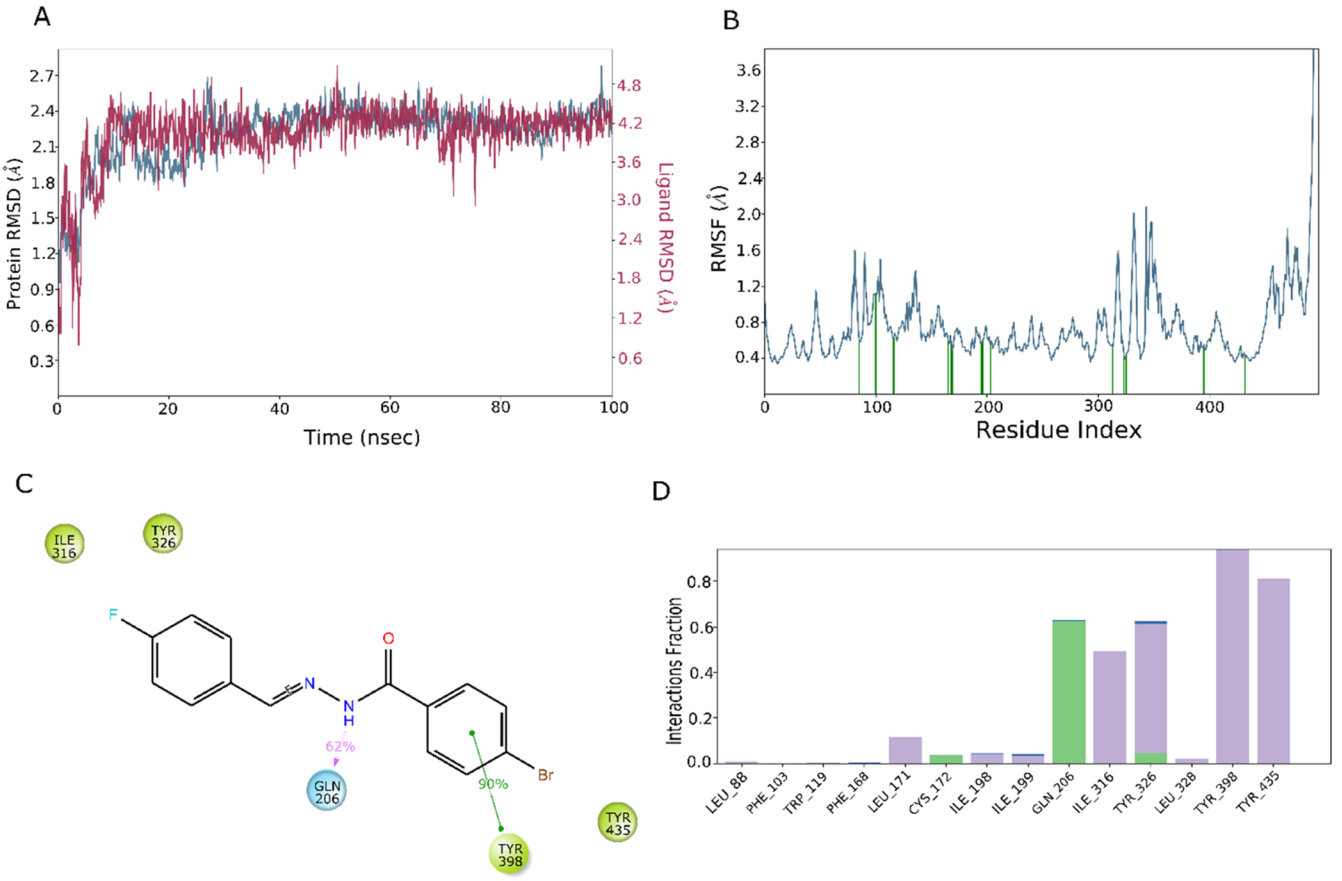

Figure 6. MD simulation analysis of the **ACH10**-MAO-B complex. (A) RMSD (protein RMSD is shown in blue, while **ACH10** RMSD is shown in red). (B) Individual RMSF for amino acids. (C) Diagram of 2D interaction. (D) Examining the protein−ligand interactions along the MD pathway. MD: molecular dynamics; RMSD: root-mean-square deviation; RMSF: root-mean-square fluctuation.

type, from 51.83% to 95.02%) and distinct from pargyline (irreversible type, from 21.83 to 22.22%). The findings presented above demonstrated that **ACH10** and **ACH14** were reversible inhibitors of MAO-B.

3.5. BBB Permeability Assay. The PAMPA was performed to assess the brain penetration for the lead compounds **ACH10** and **ACH14**. Both compounds showed considerable CNS bioavailability and permeability with Pe values greater than 4.0×10^{-6} cm/s (Table 2). For CNS drugs to be delivered effectively, brain penetration is a key requirement. Based on the calculated Pe, molecules were classified as potentially non-BBB permeable (CNS−) if the value was less than 2.0×10^{-6} cm/s, and as potentially permeable (CNS+) if the value was greater than 4.0×10^{-6} cm/s. Compounds **ACH10** and **ACH14** were observed to penetrate the BBB with their respective Pe values of 5.12×10^{-6} and 4.98×10^{-6} cm/s.

3.6. Molecular Docking. We performed molecular docking of the hit molecule within the interaction gorge of MAO-B protein 2V5Z using the Glide module. The docking scores (XP mode) for the lead compounds (**ACH10** and **ACH14**) were roughly −10.080 and 9.402 kcal/mol, respectively, while safinamide had a comparable score (−11.6837 kcal/mol). Hydrophobic interactions with Phe99, Pro102, Phe103, Phe104, Tyr60, Tyr435, Tyr398, Leu164, Phe168, Tyr326, Leu328, Leu171, Cys172, Ile198, and Ile199 were among the more significant interactions. Ring A possessed a halogen at the fourth position that was involved in the interaction with the entrance cavity of the protein. Figure 5 displays the 2D interaction diagram for hit compound **ACH10**.

3.7. Molecular Dynamics. The MD simulation is used in the investigation for discovering novel drugs to replicate the dynamic behaviors of a protein−ligand complex as accurately or realistically as feasible. This enables scientists to swiftly assimilate kinetic information regarding interactions between proteins and ligands. In this study, MD modeling in biological environments was employed to replicate **ACH10** at the active gorge of the MAO-B protein. Using the MD trajectories, the RMSD, RMSF, and protein−ligand interactions were enumerated. The RMSD value derived from the MD simulation trajectory is a vital parameter for discerning various structural arrangements of the protein backbone as the system reaches equilibrium. Figure 6 displays various MD trajectory data analyses for the ACH10-MAO-B complex. Water molecules were used to simulate both complexes. The RMSD figure (Figure 6A) demonstrated a stable protein−ligand complex during the course of the simulation, with RMSD values for protein Cα atoms in the complex with the ligand ranging from 0.95 to 2.78 Å. The ligand RMSD ranged from 1.04 to 4.45 Å for **ACH10** with respect to that of the protein. The simulation RMSD for the protein was discovered to be constant, except for a minor change: a maximum of 2.7 Å at 98 ns. At 50 ns, when the RMSD value was 5.08 Å, the maximum ligand RMSD was recorded; however, by 70 ns, it had stabilized. Overall, the ligand stability with respect to the protein and its

https://doi.org/10.1021/acsomega.3c05719
ACS Omega 2023, 8, 47606−47615

binding site was shown by the RMSD plot. The RMSF serves as a tool for assessing the flexibility and movement of particular amino acids, as illustrated in Figure 6B. Observing a decline in the RMSF value may reasonably suggest that the concerned residue has diminished activity and mobility. It is conceivable that a stronger protein−ligand interaction is achieved when the RMSF value is low for residues located near the active site or those participating in the interaction between the ligand and the receptor protein. The N- and C-terminal residues exhibited significantly higher fluctuations (0.33−7.05 Å) and significantly fewer fluctuations (0.33−7.05 Å), respectively, according to the RMSF plot (Figure 6B). The 14 amino acid residues with which the ligand interacted were Phe103 (1.12 Å), Trp119 (0.62 Å), Phe168 (0.602 Å), Ile199 (0.59 Å), Leu88 (0.58 Å), Ile198 (0.57 Å), Leu171 (0.564 Å), Gln206 (0.55 Å), Tyr398 (0.55 Å), Ile316 (0.52 Å), Cys172 (0.48 Å), Leu328 (0.44 Å), Tyr326 (0.43 Å), and Tyr435 (0.39 Å). Some claims suggest that hydrogen bonding is a pivotal factor in the field of drug development, contributing to our comprehension of the metabolism, absorption, and selectivity. Noncovalent interactions, such as hydrophobic, π−cation, π−π, and polar or ionic interactions as well as the formation of water-bridge hydrogen bonds, have proven to be instrumental in revealing the dynamics of protein−ligand conformations throughout the course of MD simulations. Tyr398, Tyr435, Ile316, Tyr326, and Leu171 showed hydrophobic interactions with high frequency. Gln206 and Cys172 showed a hydrogen-bonding interaction. In ligand−protein complexes, hydrogen bonds, water bridges, and hydrophobic stability are shown in Figure 6C,D. Tyr398 participated in a 90% pi-pi stack contact with Gln206, which formed a hydrogen bond with the NH atom of the hydrazide group of **ACH10** with a 62% strength. The more accurate reproduction of the physiological milieu in molecular dynamics simulations will facilitate the comprehension of the binding patterns. The trajectory analysis and complete MD simulation predict that the lead chemical will inhibit MAO-B.

4. CONCLUSIONS

We synthesized acyl hydrazine derivatives and evaluated their efficacy as inhibitors of MAOs. Every acyl hydrazine that was synthesized had a substantial MAO-B inhibiting effect. Notably, MAO-B inhibitors **ACH10** (IC_{50} = 0.14 μM) and **ACH14** (IC_{50} = 0.15 μM) exhibited significant potency. Both of these compounds acted as competitive and reversible inhibitors of MAO-B. Docking studies determined hydrophobic interactions of the lead chemical compound **ACH10** with an MAO-B protein residue. The simulated study revealed that both pi−pi interactions and hydrogen bonds play major roles in maintaining the stability of the **ACH10**-MAO-B complex. These results highlighted the potential of **ACH10** and **ACH14** in treating neurological conditions including PD.

■ ASSOCIATED CONTENT

Supporting Information

The Supporting Information is available free of charge at https://pubs.acs.org/doi/10.1021/acsomega.3c05719.

Spectral data of ^{1}H- and ^{13}C NMR and HRMS chromatograms for compounds; **ACH1−ACH14** (PDF)

■ AUTHOR INFORMATION

Corresponding Authors

Subin Mary Zachariah − *Department of Pharmaceutical Chemistry, Amrita School of Pharmacy, Amrita Vishwa Vidyapeetham, Kochi 682 041, India*; Email: subinmaryzachariah@aims.amrita.edu

Hoon Kim − *Department of Pharmacy, and Research Institute of Life Pharmaceutical Sciences, Sunchon National University, Suncheon 57922, Republic of Korea*; orcid.org/0000-0002-7203-3712; Email: hoon@sunchon.ac.kr

Bijo Mathew − *Department of Pharmaceutical Chemistry, Amrita School of Pharmacy, Amrita Vishwa Vidyapeetham, Kochi 682 041, India*; orcid.org/0000-0002-6658-4497; Email: bijomathew@aims.amrita.edu, bijovilaventgu@gmail.com

Authors

Jayalakshmi Jayan − *Department of Pharmaceutical Chemistry, Amrita School of Pharmacy, Amrita Vishwa Vidyapeetham, Kochi 682 041, India*

Jiseong Lee − *Department of Pharmacy, and Research Institute of Life Pharmaceutical Sciences, Sunchon National University, Suncheon 57922, Republic of Korea*

Sunil Kumar − *Department of Pharmaceutical Chemistry, Amrita School of Pharmacy, Amrita Vishwa Vidyapeetham, Kochi 682 041, India*

Amritha Manoharan − *Department of Pharmaceutical Chemistry, Amrita School of Pharmacy, Amrita Vishwa Vidyapeetham, Kochi 682 041, India*

Anishma Payyappilliparambil Narayanan − *Department of Pharmaceutical Chemistry, Amrita School of Pharmacy, Amrita Vishwa Vidyapeetham, Kochi 682 041, India*

Reenoo Jauhari − *School of Pharmacy, Graphic Era Hill University, Dehradun 248002 Uttarakhand, India*

Mohamed A. Abdelgawad − *Department of Pharmaceutical Chemistry, College of Pharmacy, Jouf University, Sakaka 72341, Saudi Arabia; Pharmaceutical Organic Chemistry Department, Faculty of Pharmacy, Beni-Suef University, Beni Suef 62514, Egypt*

Mohammed M. Ghoneim − *Department of Pharmacy Practice, College of Pharmacy, AlMaarefa University, Riyadh 13713, Saudi Arabia; Pharmacognosy and Medicinal Plants Department, Faculty of Pharmacy, Al-Azhar University, Cairo 11884, Egypt*

Hasnaa Ali Ebrahim − *Department of Basic Medical Sciences, College of Medicine, Princess Nourah bint Abdulrahman University, Riyadh 11671, Saudi Arabia*

Complete contact information is available at: https://pubs.acs.org/10.1021/acsomega.3c05719

Author Contributions

◆J.J. and J.L. contributed equally to this work.

Notes

The authors declare no competing financial interest.

■ ACKNOWLEDGMENTS

This work was funded by Princess Nourah bint Abdulrahman University Researchers Supporting Project number (PNURSP2023R171), Princess Nourah bint Abdulrahman University, Riyadh, Saudi Arabia.

REFERENCES

(1) Rojas, R. J.; Edmondson, D. E.; Almos, T.; Scott, R.; Massari, M. E. Reversible and irreversible small molecule inhibitors of monoamine oxidase B (MAO-B) investigated by biophysical techniques. *Bioorg. Med. Chem.* **2015**, *23*, 770−778.

(2) Behl, T.; Kaur, D.; Sehgal, A.; Singh, S.; Sharma, N.; Zengin, G.; Andronie-Cioara, F. L.; Toma, M. M.; Bungau, S.; Bumbu, A. G. Role of monoamine oxidase activity in Alzheimer's disease: An insight into the therapeutic potential of inhibitors. *Molecules* **2021**, *26*, No. 3724, DOI: 10.3390/molecules26123724.

(3) Robinson, S. J.; Petzer, J. P.; Petzer, A.; Bergh, J. J.; Lourens, A. C. U. Selected furanochalcones as inhibitors of monoamine oxidase. *Bioorg. Med. Chem. Lett.* **2013**, *23*, 4985−4989.

(4) Guglielmi, P.; Mathew, B.; Secci, D.; Carradori, S. Chalcones: Unearthing their therapeutic possibility as monoamine oxidase B inhibitors. *Eur. J. Med. Chem.* **2020**, *205*, No. 112650.

(5) Dugger, B. N.; Dickson, D. W. Pathology of neurodegenerative diseases. *Cold Spring Harbor Perspect. Biol.* **2017**, *9*, No. a028035, DOI: 10.1101/cshperspect.a028035.

(6) Soria Lopez, J. A.; González, H. M.; Léger, G. C. Alzheimer's Disease. In *Handbook of Clinical Neurology*; Elsevier, 2019; pp 231−255.

(7) Ramsay, R. R. Monoamine oxidases: The biochemistry of the proteins as targets in medicinal chemistry and drug discovery. *Curr. Top. Med. Chem.* **2012**, *12*, 2189−2209, DOI: 10.2174/156802612805219978.

(8) Youdim, M. B. H.; Bakhle, Y. S. Monoamine oxidase: isoforms and inhibitors in Parkinson's disease and depressive illness. *Br. J. Pharmacol.* **2006**, *147*, S287−S296, DOI: 10.1038/sj.bjp.0706464.

(9) Saura, J.; Luque, J. M.; Cesura, A. M.; Prada, M. D.; Chan-Palay, V.; Huber, G.; Löffler, J.; Richards, J. G. Increased monoamine oxidase b activity in plaque-associated astrocytes of Alzheimer brains revealed by quantitative enzyme radioautography. *Neuroscience* **1994**, *62*, 15−30.

(10) Imbimbo, B. P.; Watling, M. Investigational BACE inhibitors for the treatment of Alzheimer's disease. *Expert Opin. Invest. Drugs* **2019**, *28*, 967−975.

(11) Tipton, K. F. 90 years of monoamine oxidase: some progress and some confusion. *J. Neural Transm.* **2018**, *125*, 1519−1551, DOI: 10.1007/s00702-018-1881-5.

(12) Lum, C. T.; Stahl, S. M. Opportunities for reversible inhibitors of monoamine oxidase-A (RIMAs) in the treatment of depression. *CNS Spectr.* **2012**, *17*, 107−120.

(13) Elshaflu, H.; Todorović, T. R.; Nikolić, M.; Lolić, A.; Višnjevac, A.; Hagenow, S.; Padrón, J. M.; García-Sosa, A. T.; Djordjević, I. S.; Grubišić, S.; Stark, H.; Filipović, N. R. Selenazolyl-hydrazones as novel selective MAO inhibitors with antiproliferative and antioxidant activities: Experimental and *in-silico* studies. *Front. Chem.* **2018**, *6*, No. 247, DOI: 10.3389/fchem.2018.00247.

(14) Moussa-Pacha, N. M.; Abdin, S. M.; Omar, H. A.; Alniss, H.; Al-Tel, T. H. BACE1 inhibitors: Current status and future directions in treating Alzheimer's disease. *Med. Res. Rev.* **2020**, *40*, 339−384.

(15) Mathew, B.; Uçar, G.; Mathew, G. E.; Mathew, S.; Purapurath, P. K.; Moolayil, F.; Mohan, S.; Gupta, S. V. Monoamine oxidase inhibitory activity: Methyl-versus chlorochalcone derivatives. *ChemMedChem* **2016**, *11*, 2649−2655.

(16) Mathew, B.; Ucar, G.; Yabanogclu-Ciftci, S.; Baysal, I.; Suresh, J. A.; Mathew, G. E.; Vilapurathu, J. K.; Nadeena, A. M.; Nabeela, P.; Lakshmi, V.; Haridas, A.; Fathima, F. Development of fluorinated thienylchalcones as monoamine oxidase-B inhibitors: Design, synthesis, biological evaluation and molecular docking studies. *Lett. Org. Chem.* **2015**, *12*, 605−613, DOI: 10.2174/1570178612666150903213416.

(17) Iacovino, L. G.; Pinzi, L.; Facchetti, G.; Bortolini, B.; Christodoulou, M. S.; Binda, C.; Rastelli, G.; Rimoldi, I.; Passarella, D.; Paolo, M. L. D.; Via, L. D. Promising non-cytotoxic monosubstituted chalcones to target monoamine oxidase-B. *ACS Med. Chem. Lett.* **2021**, *12*, 1151−1158.

(18) Mellado, M.; Salas, C. O.; Uriarte, E.; Viña, D.; Jara-Gutiérrez, C.; Matos, M. J.; Cuellar, M. Design, synthesis and docking calculations of prenylated chalcones as selective monoamine oxidase B inhibitors with antioxidant activity. *ChemistrySelect* **2019**, *4*, 7698−7703.

(19) Koyiparambath, V. P.; Rajappan, K. P.; Rangarajan, T. M.; Al-Sehemi, A. G.; Pannipara, M.; Bhaskar, V.; Nair, A. S.; Sudevan, S. T.; Kumar, S.; Mathew, B. Deciphering the detailed structure−activity relationship of coumarins as monoamine oxidase enzyme inhibitors—An updated review. *Chem. Biol. Drug Des.* **2021**, *98*, 655−673, DOI: 10.1111/cbdd.13919.

(20) Kumar, S.; Nair, A. S.; Abdelgawad, M. A.; Mathew, B. Exploration of the detailed structure−activity relationships of isatin and their isomers as monoamine oxidase inhibitors. *ACS Omega* **2022**, *7*, 16244−16259.

(21) Królicka, E.; Kieć-Kononowicz, K.; Łażewska, D. Chalcones as potential ligands for the treatment of Parkinson's disease. *Pharmaceuticals* **2022**, *15*, No. 847, DOI: 10.3390/ph15070847.

(22) Tripathi, R. K. P.; Ayyannan, S. R. Design, synthesis, and evaluation of 2-amino-6-nitrobenzothiazole-derived hydrazones as MAO inhibitors: Role of the methylene spacer group. *ChemMedChem* **2016**, *11*, 1551−1567.

(23) Tok, F.; Sağlık, B. N.; Özkay, Y.; Ilgın, S.; Kaplancıklı, Z. A.; Koçyiğit-Kaymakçıoğlu, B. Synthesis of new hydrazone derivatives and evaluation of their monoamine oxidase inhibitory activity. *Bioorg. Chem.* **2021**, *114*, No. 105038.

(24) Salgin-Goksen, U.; Telli, G.; Erikci, A.; Dedecengiz, E.; Tel, B. C.; Kaynak, F. B.; Yelekci, K.; Ucar, G.; Gokhan-Kelekci, N. New 2-pyrazoline and hydrazone derivatives as potent and selective monoamine oxidase A inhibitors. *J. Med. Chem.* **2021**, *64*, 1989−2009.

(25) Bolognino, I.; Giangregorio, N.; Tonazzi, A.; Martínez, A. L.; Altomare, C. D.; Loza, M. I.; Sablone, S.; Cellamare, S.; Catto, M. Synthesis and biological evaluation of dantrolene-like hydrazide and hydrazone analogues as multitarget agents for neurodegenerative diseases. *ChemMedChem* **2021**, *16*, 2807−2816.

(26) de Freitas Silva, M.; Lima, E. T.; Pruccoli, L.; Castro, N.; Guimarães, M.; da Silva, F.; Nadur, N. F.; de Azevedo, L.; Kümmerle, A.; Guedes, I.; Dardenne, L.; Gontijo, V.; Tarozzi, A.; Viegas, C. Design, synthesis and biological evaluation of novel triazole N-acylhydrazone hybrids for Alzheimer's disease. *Molecules* **2020**, *25*, No. 3165, DOI: 10.3390/molecules25143165.

(27) Dézsi, L.; Vécsei, L. Safinamide for the treatment of Parkinson's disease. *Expert Opin. Invest. Drugs* **2014**, *23*, 729−742.

(28) Mathew, B.; Carradori, S.; Guglielmi, P.; Uddin, M. S.; Kim, H. New aspects of monoamine oxidase B inhibitors: The key role of halogens to open the golden door. *Curr. Med. Chem.* **2020**, *28*, 266−283.

(29) Abid, S. M. A.; Younus, H. A.; Al-Rashida, M.; Arshad, Z.; Maryum, T.; Gilani, M. A.; Alharthi, A. I.; Iqbal, J. Sulfonyl hydrazones derived from 3-formylchromone as non-selective inhibitors of MAO-A and MAO-B: Synthesis, molecular modelling and *in-silico* ADME evaluation. *Bioorg. Chem.* **2017**, *75*, 291−302, DOI: 10.1016/j.bioorg.2017.10.001.

(30) Oh, J. M.; Rangarajan, T. M.; Chaudhary, R.; Singh, R. P.; Singh, M.; Singh, R. P.; Tondo, A. R.; Gambacorta, N.; Nicolotti, O.; Mathew, B.; Kim, H. Novel class of chalcone oxime ethers as potent monoamine oxidase-B and acetylcholinesterase inhibitors. *Molecules* **2020**, *25*, No. 2356, DOI: 10.3390/molecules25102356.

(31) Taghavi, A.; Nasir, S.; Pickhardt, M.; Heyny-von Haussen, R.; Mall, G.; Mandelkow, E.; Mandelkow, E. M.; Schmidt, B. N'-benzylidene-benzohydrazides as novel and selective tau-PHF ligands. *J Alzheimers Dis.* **2011**, *27* (4), 835−843.

(32) Arya, N.; Mishra, S. K.; Suryaprakash, N. Intramolecular hydrogen bond directed distribution of conformational populations in the derivatives of N′-benzylidenebenzohydrazide. *New J. Chem.* **2019**, *43* (33), 13134−13142.

(33) Lee, H. W.; Ryu, H. W.; Kang, M. -G.; Park, D.; Lee, H.; Shin, H. M.; Oh, S. -R.; Kim, H. Potent inhibition of monoamine oxidase A

https://doi.org/10.1021/acsomega.3c05719
ACS Omega 2023, 8, 47606−47615

by decursin from *Angelica gigas* Nakai and by wogonin from *Scutellaria baicalensis* Georgi. *Int. J. Biol. Macromol.* **2017**, *97*, 598−605.
(34) Oh, J. M.; Kang, Y.; Hwang, J. H.; Park, J. -H.; Shin, W. -H.; Mun, S. -K.; Lee, J. U.; Yee, S. -T.; Kim, H. Synthesis of 4-substituted benzyl-2-triazole-linked-tryptamine-paeonol derivatives and evaluation of their selective inhibitions against butyrylcholinesterase and monoamine oxidase-B. *Int. J. Biol. Macromol.* **2022**, *217*, 910−921.
(35) Baek, S. C.; Park, M. H.; Ryu, H. W.; Lee, J. P.; Kang, M. -G.; Park, D.; Park, C. M.; Oh, S. -R.; Kim, H. Rhamnocitrin isolated from *Prunus padus* var. seoulensis: A potent and selective reversible inhibitor of human monoamine oxidase A. *Bioorg. Chem.* **2019**, *83*, 317−325.
(36) Baek, S. C.; Lee, H. W.; Ryu, H. W.; Kang, M. -G.; Park, D.; Kim, S. H.; Cho, M. -L.; Oh, S. -R.; Kim, H. Selective inhibition of monoamine oxidase A by hispidol. *Bioorg. Med. Chem. Lett.* **2018**, *28*, 584−588.
(37) Oh, J. M.; Jang, H. -J.; Kim, W. J.; Kang, M. -G.; Baek, S. C.; Lee, J. P.; Park, D.; Oh, S. -R.; Kim, H. Calycosin and 8-*O*-methylretusin isolated from *Maackia amurensis* as potent and selective reversible inhibitors of human monoamine oxidase-B. *Int. J. Biol. Macromol.* **2020**, *151*, 441−448.
(38) Lee, H. W.; Ryu, H. W.; Kang, M. -G.; Park, D.; Oh, S. -R.; Kim, H. Potent selective monoamine oxidase B inhibition by maackiain, a pterocarpan from the roots of *Sophora flavescens*. *Bioorg. Med. Chem. Lett.* **2016**, *26*, 4714−4719.
(39) Mathew, B.; Haridas, A.; Uçar, G.; Baysal, I.; Joy, M.; Mathew, G. E.; Lakshmanan, B.; Jayaprakash, V. Synthesis, biochemistry, and computational studies of brominated thienyl chalcones: A new class of reversible MAO-B inhibitors. *ChemMedChem* **2016**, *11*, 1161−1171.
(40) Parambi, D. G. T.; Oh, J. M.; Baek, S. C.; Lee, J. P.; Tondo, A. R.; Nicolotti, O.; Kim, H.; Mathew, B. Design, synthesis and biological evaluation of oxygenated chalcones as potent and selective MAO-B inhibitors. *Bioorg. Chem.* **2019**, *93*, No. 103335.
(41) Vishal, V. P.; Oh, J. M.; Khames, A.; Abdelgawad, M. A.; Nair, A. S.; Nath, L. R.; Gambacorta, N.; Ciriaco, F.; Nicolotti, O.; Kim, H.; Mathew, B. Trimethoxylated halogenated chalcones as dual inhibitors of MAO-B and BACE-1 for the treatment of neurodegenerative disorders. *Pharmaceutics* **2021**, *13*, No. 850, DOI: 10.3390/pharmaceutics13060850.
(42) Shaw Research D. E.. *Schrodinger Release Desmond molecular dynamics system. Maestro Desmond Interoperability Tools*, 2022.
(43) Ayipo, Y. O.; Alananzeh, W. A.; Ahmad, I.; Patel, H.; Mordi, M. N. Structural modelling and *in silico* pharmacology of *β*-carboline alkaloids as potent 5-HT1A receptor antagonists and reuptake inhibitors. *J. Biomol. Struct. Dyn.* **2023**, *41*, 6219−6235.
(44) Farhan, M. M.; Guma, M. A.; Rabeea, M. A.; Ahmad, I.; Patel, H. Synthesizes, characterization, molecular docking and in vitro bioactivity study of new compounds containing triple beta lactam rings. *J. Mol. Struct.* **2022**, *1269*, No. 133781.
(45) Radwan, H. A.; Ahmad, I.; Othman, I. M. M.; Gad-Elkareem, M. A. M.; Patel, H.; Aouadi, K.; Snoussi, M.; Kadri, A. Design, synthesis, in vitro anticancer and antimicrobial evaluation, SAR analysis, molecular docking and dynamic simulation of new pyrazoles, triazoles and pyridazines based isoxazole. *J. Mol. Struct.* **2022**, *1264*, No. 133312.
(46) Finberg, J. P. M.; Rabey, J. M. Inhibitors of MAO-A and MAO-B in psychiatry and neurology. *Front. Pharmacol.* **2016**, *7*, No. 340, DOI: 10.3389/fphar.2016.00340.
(47) Mostert, S.; Petzer, A.; Petzer, J. P. Indanones as high-potency reversible inhibitors of monoamine oxidase. *ChemMedChem* **2015**, *10* (5), 862−873.

https://doi.org/10.1021/acsomega.3c05719
ACS Omega 2023, 8, 47606−47615